

Modeling of Elastic Behavior of 3D Deformable Objects from Range and Tactile Imaging

Ana-Maria Cretu, Pierre Payeur, and Emil M. Petriu

University of Ottawa, SITE, 800 King Edward,
Ottawa, ON, K1N6N5, Canada
{acretu,ppayeur,petriu}@site.uottawa.ca

Abstract. The paper presents a joint sensing strategy that combines tactile probing and range imaging for the mapping of the elastic properties that characterize 3D deformable objects. A feedforward neural network architecture is employed in an original manner to model the complex relationship between the surface deformation and the forces exemplified in non-rigid bodies. Experimental results are presented for objects made of materials with different elastic behaviors and for their different deformation stages.

Keywords: Deformable objects, elastic behavior, range imaging, tactile probing, neural networks.

1 Introduction

The problem of accurately modeling deformable objects is not trivial. The area of expertise required covers a vast range of topics such as: the determination of proper equipment to perform measurements, the fusion of different technologies and of data available from different sources to improve the measurement process, the interpretation, analysis and correlation of data, the proper selection of methods to model elastic data and to join these data in coherent composite geometric and elastic models, and finally the means of interacting with the models. While an intensive research has been performed on several of these topics in the past decades, the thorough literature review conducted during this research led to the conclusion that there were certain limitations and several neglected aspects related to the measurement and modeling of deformable objects.

The main limitation encountered is related to the focus of current researchers on simulations based on assumptions on the material of the deformable object and on means to interact with the increasingly complex models in real-time. Much less attention has been given to real measurements of elastic behavior, in the detriment of accuracy and realism. Overall, there are few papers that imply any sort of procedure to elicit and collect the object's elastic behavior, and in most cases when a measurement is performed, the probing is limited to a single point. Such an approach can only produce satisfactory results for objects made of homogeneous elastic materials and is unsuitable for heterogeneous or piecewise homogeneous objects. Moreover, many of the proposed solutions are highly specialized and dedicated to a particular application and cannot be employed in a different context. These are some of the reasons that drove the research work presented in this paper.

2 Related Work

The most popular solutions to collect elastic measurements in daily engineering problems are indentation and vision-based measurements. A series of images of an object before and after the deformation are analyzed individually and profiles are extracted in order to compute displacements. Wang *et al.* [1] use a grid of markers and employ corner extraction to obtain the coordinates of various feature points in the grid and their displacement. A similar idea is exploited by Kamiyama *et al.* [2], whose tactile sensor has a transparent elastic body with markers. By taking images of a certain marker in the interior of the body, the variation information of the interior is measured when a force is applied to the surface of an object. Vuskovic *et al.* [3] use a specially designed instrument to measure hyperelastic, isotropic materials based on pipette tissue aspiration. The deformation is captured by a camera and the material parameters are determined using the inverse finite element method (FEM) from the collected images. The sensor of Ferrier *et al.* [4] and Hristu *et al.* [5] consists of an elliptical membrane, filled with fluid-like gel and inscribed with a grid of dots at precise locations. Images of the grid taken as the membrane deforms are used to reveal the elastic properties. Greminger *et al.* [6] take images after and before deformation to train a neural network that defines the deformation of an elastic object submitted to an external force.

However, the majority of these methods are based on assumptions on the objects' material. As an improvement from our previous work on this research topic [7], this paper discusses a general purpose scheme for measuring and representing elastic behavior of deformable objects without *a priori* knowledge on the material that the objects under study are made of.

3 Proposed Modeling Scheme

The proposed approach does not attempt to recover explicitly neither the elastic constants, nor the stress and strain tensors. The procedure of recovery of elastic parameters and stress and strain tensors implies complicated mathematical models based on assumptions. Such models are frequently impossible to define and solve for highly nonlinear elastic materials. The focus in this work is on the observation of the displacement of the surface of an object when loaded by a measured external force.

The mapping between the deformation profiles and forces is learned inherently using neural networks. Such an approach avoids the complex and time consuming methods to recuperate elastic parameters from experimental data and any assumptions on the material under study that such methods imply. A feedforward neural network is employed to model the elastic behavior of selected sample points that are probed simultaneously by a force/torque sensor and an active range finder. Therefore the proposed framework allows not only to infer the elastic parameters at the sampled points by learning the mapping from force to deformation profiles respectively, but also to provide an estimate on the elastic behavior on surrounding points that are not part of the selected sampling point set. Moreover, the fault-tolerant nature of neural networks improves the behavior of the proposed modeling scheme in the presence of

noise inherent in any real measurement data. The same neural network architecture with the same parameters can be used as long as the measurements are collected with the same equipment (same number of sample points in the profiles and/or curves). This eliminates the need for an expert user to make the necessary adjustments for each material to be modeled.

3.1 Experimental Setup and Test Objects

The experimental setup used to collect force and deformation data is depicted in Fig. 1a. It comprises a multi-axis *ATI* force/torque sensor attached to a console computer, and an active triangulation line-scanning Jupiter laser range finder attached to a second computer.

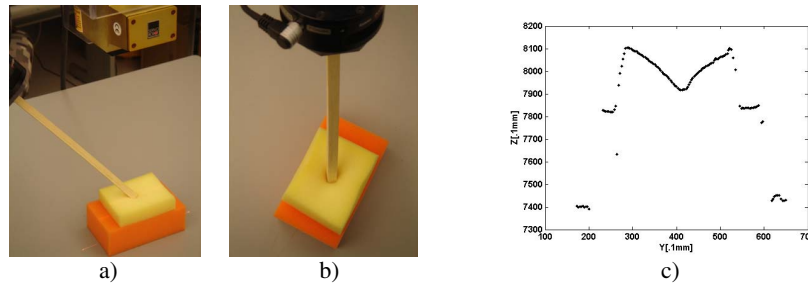


Fig. 1. a) Range sensor and b) force/torque setup producing a laser trace to capture the object deformation profile resulting from the applied force, and c) deformation profile in the Y - Z space

During the probing procedure, guided by the algorithm proposed in [7], the force/torque sensor records the force components applied on the object, while the range finder captures the deformation profile of the surface of the object under a given load. The range finder is placed above the object under study such that the scan-line intersects with the point where the external force is applied, as highlighted by the trace of the laser on the object in Fig. 1b. The raw deformation profiles collected from the range finder are encoded under the form of 2D distributions of points in the Y - Z space, as shown in Fig. 1c, where Y is the lateral displacement along the scan-line and Z the depth along the optical axis with respect to a back reference plane.

The laser range finder provides fast scans of 512 samples distributed along a straight line on the surface. A number of 75 to 100 scans of the same area are collected within a few seconds while the interaction parameters (e.g. the force magnitude, the angle at which the force is applied, the orientation of the range finder and the point where the force is applied) are kept constant. In order to filter out the average noise and include as many valid measurements as possible in areas where points could be missing in some of the scans, the mean value is computed on the depth (Z -axis) over all deformation profiles obtained for a given set of interaction parameters. The resulting profiles are saved for each magnitude and angle of force applied at each probed point of an object at different orientations of the range finder.

3.2 Elastic Behavior Characterization

In order to prove that the proposed framework operates from noisy experimental measurements without *a priori* knowledge on the material of the object under study, raw data collected on a set of representative objects with different elastic behaviors, as depicted in Fig. 2, is used for experimentation.



Fig. 2. Objects used for experimentation: a) battery, b) cardboard cup, and c) foam sponges

A simple way to detect the cases when a plastic or elasto-plastic deformation occurs is to compare the initial profile collected in the beginning of the measurement procedure, before any force is applied, with the deformation profile when the last force is applied, and with the final deformation profile after all interacting forces are removed from the surface of an object, as shown in Fig. 3.

The majority of objects exhibit an elastic behavior for small magnitudes of forces, meaning that the object restores its shape after the force is removed, as in the first row of Fig. 3. When the magnitude of the applied force is increased, the object passes into its elasto-plastic stage depicted in the second row of Fig. 3. A certain amount of plastic deformation occurs after the removal of the last deformation force. The object restores its shape only partially when all external forces are removed.

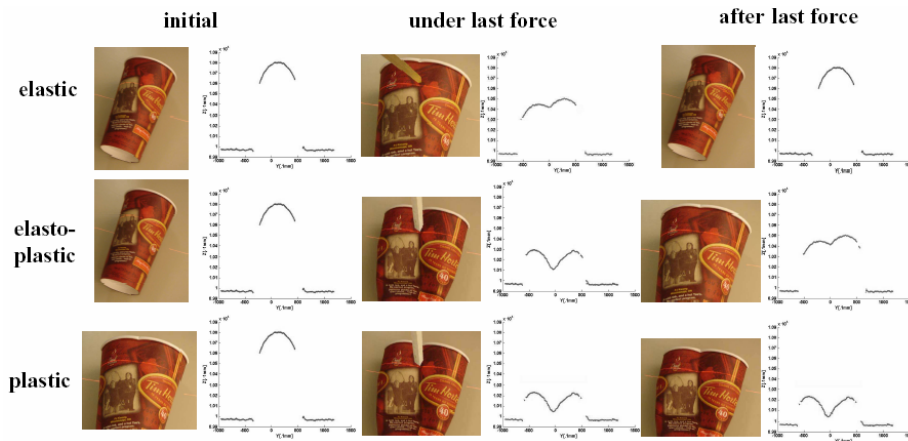


Fig. 3. Deformation profiles for elastic, plastic and elasto-plastic materials in various deformation stages

When the magnitude of force is further increased, a permanent plastic behavior occurs, as shown in the third row of Fig. 3. The object remains in the same shape that it was when the last force applied was still acting on it.

These observations suggest that a simple way to detect if a plastic or elasto-plastic deformation occurs is to compare at first the initial and final deformation profiles. If these are different (more than a threshold that covers for the noise in the measurements), it means that either a plastic or an elasto-plastic behavior occurred. The distinction between the plastic and elasto-plastic behaviors can be made by comparing the final deformation profile with the one resulting from the application of the last force on the object. If they are identical within reasonable noise limits, it implies that a plastic deformation occurred. If they are different, the material exhibits elasto-plastic properties or the object is within its elasto-plastic deformation stage.

3.3 Elastic Behavior Modeling

A feedforward neural network is employed to learn the relation between the parameters recorded during the interaction with the object and the corresponding deformation profiles provided by the range finder. The network has six input neurons associated with the interaction parameters namely: the magnitude of force (F), the angle (a) of the applied force, the orientation of the range finder (p) with respect to the object, the coordinates of the point (u, v, w) where the force is applied with respect to the object, and the deformation stage (s). 45 hidden neurons (H_1 - H_{45}) are used and the output vector has the same size as the length of the deformation profile (Z), as shown in Fig. 4.

The parameter s refers to the state of the material described in the previous section. The elastic deformation stage of any object is characterized by $s=0$, the elasto-plastic stage by $s=0.5$ and the plastic one by $s=1$. The tagging of data for the different deformation stages or different material states is done during the data collection

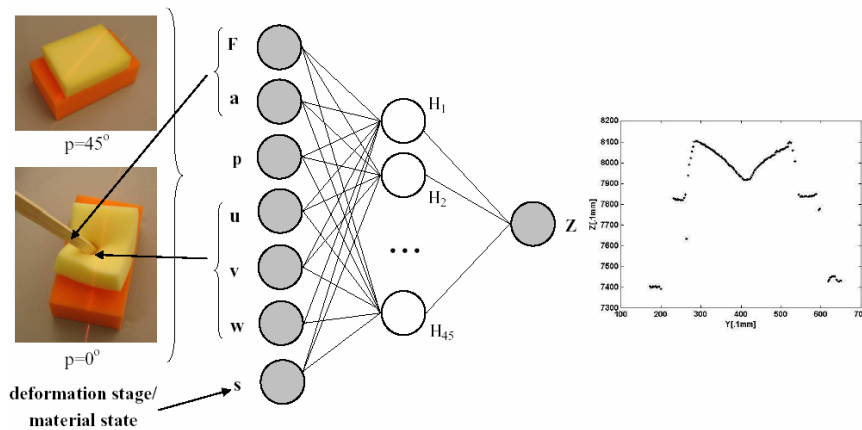


Fig. 4. Neural network to model elastic, elasto-plastic and plastic deformation stages

procedure by continuously monitoring the differences between the initial profile, the final profile and the profile obtained when the last force was applied.

The only data preprocessing applied on the collected deformation profiles is a normalization of the depth data contained in the deformation profiles to the $[0 \ 1]$ interval prior to training. By experimentation, a number of 45 hidden neurons gave a good compromise between the accuracy of modeling and the length of training. The network for each object under study is trained for 20000 epochs using the resilient propagation algorithm, with the learning rate set to 0.1. The training takes approximately 5 min. on a Pentium IV 1.3GHz machine with 512MB memory. Once trained, the network takes as inputs the interaction parameters (F , a , p , u , v , w , s) and outputs the corresponding deformation profile as an indexed vector of depth values, Z , along the scan-line.

4 Experimental Results

Experiments are performed for all objects presented in Fig. 2. The case of rigid objects is exemplified by the battery in Fig. 2a, whose measured deformation profiles and modeling results for different forces applied in the normal direction and at different range finder orientations are depicted in Fig. 5.

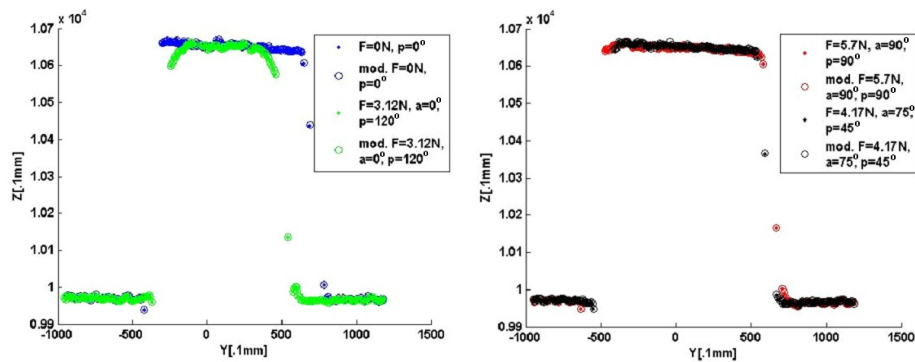


Fig. 5. Rigid object: real and modeled data

The measured profiles represent the raw profiles collected by the range finder for different values of the interaction parameters (F , a , p , u , v , w , s), while the modeled profiles are obtained at the output of the neural network when the same parameters as the ones used when the profile was collected are presented at its input. As it can be observed, in this case the deformation profiles do not vary much, as it is expected for a rigid object. The modeled data denoted by circles is very close to the measurement data denoted by dots.

Fig. 6 depicts modeling results for the cardboard cup in Fig. 2b. A set of control points A , B , C and D is defined in Fig. 6a for better visualization.

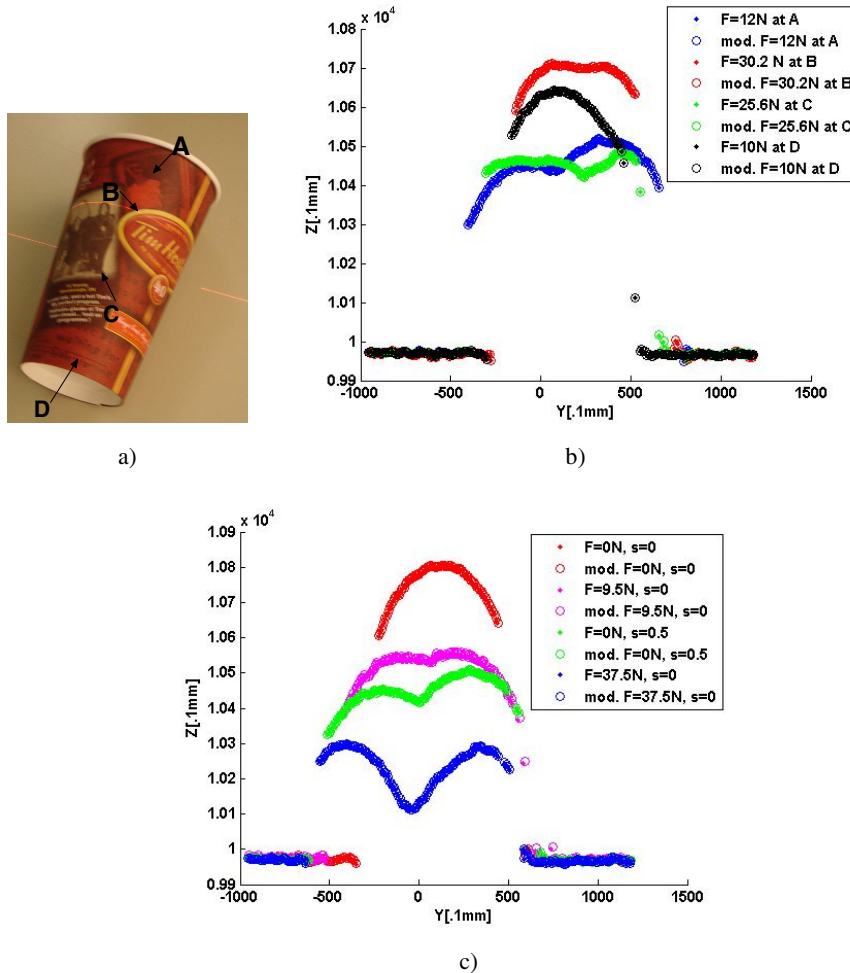


Fig. 6. (a) Control points, (b) real and modeled data for elasto-plastic object for the range finder orientation $p=90^\circ$ and different force magnitudes applied in the normal direction ($a=90^\circ$) at all control points, and c) real and modeled data for forces applied at point C

The measured and modeled deformation profiles for the cardboard cup are shown in Fig. 6b for a fixed orientation of the range finder at $p=90^\circ$ (across the width of the cup), and for forces applied perpendicular to the surface of the cup, $a=90^\circ$, on all of the predefined control points. Fig. 6c shows measured and modeled deformation profiles for the same cup modeling results at point C, with an orientation $p=90^\circ$ of the range finder and for increasing normal forces. The average mean squared error reached for the training of the neural network is 2.9×10^{-5} . It can be observed that the modeled data, depicted with circles follows closely the measurement data shown with dots in both cases.

The red, magenta and blue profiles belong to the region where the object exhibits elastic behavior. After the application of a force $F=37.5\text{N}$ (the deformation profile is shown in blue) the object enters the elasto-plastic region of deformation. The object surface does not return to the non-deformed state, but to an intermediate profile, shown in black between the non-deformed state (shown in red) and the state when the latest force was applied (shown in blue). For the deformation profile shown in black, s becomes 0.5. It can be seen that the network is able to capture the different deformation states as well, fact proven by the very similar measured and modeled data profiles.

Another interesting aspect to be noticed in Fig. 6c is that the initial non-deformed profile, shown in red is narrower along the Y axis than any of the deformed profiles. This phenomenon occurs because of a volume expansion of the object under probing, due to the applied forces. This expansion is well captured in the modeled results. Therefore the proposed method of deformation measurement and modeling using neural networks captures naturally volume expansions due to loading which are a challenge to be modeled using other methods, such as mass-spring models or FEM.

Fig. 7 presents modeling results for the set of sponges in Fig. 2c. The control points O and D are defined in Fig. 7a and an image of the sponges when a force is applied at point D is presented in Fig. 7b to enhance the visualization. Fig. 7c shows the real measurements and the modeled data provided by the proposed neural architecture at point D for different force magnitudes applied in the normal direction to the surface and for a fixed orientation of the range finder at $p=0^\circ$.

The resulting average mean squared training error, measured in mm, computed between the training and the modeled data over all the displacement curves in the training set, is 1.95×10^{-6} . The maximum mean square error encountered is 2.44×10^{-5} .

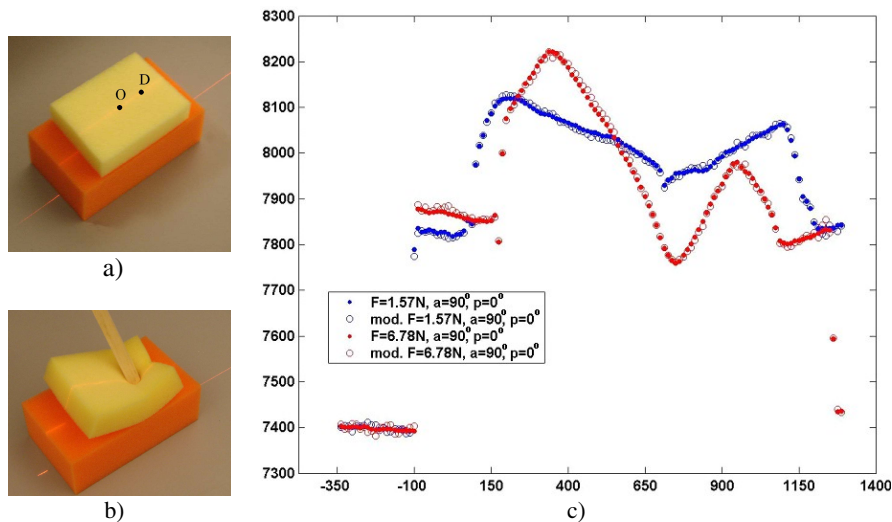


Fig. 7. Set of sponges: a) control points, b) image of sponges when a force $F=6.78\text{N}$ is applied at point D and c) real and modeled data at point D

These values show that the modeling results are very close to the training data. It can be observed that the modeled data follows closely the measurement data even for large nonlinear deformations such as those that occur in the case of the foam sponges.

Additional testing is performed to evaluate the generalization capabilities of the modeling scheme, by presenting to the neural network data that were not part of the training set. Fig. 8 shows real, modeled and estimated deformation profiles for a constant force of $F=7.5N$ applied at normal direction to the surface ($\alpha=90^\circ$) on point O defined in Fig. 7a and for different orientations of the range finder. The estimated profiles are provided by the neural network as response to an input sequence of interaction parameters that was not used for training. In this example the network is tested for orientations of the range finder that were not part of the training set.

Modeled and real data are presented from two viewpoints, lateral in Fig. 8a and top in Fig. 8b to better show the results. The estimated profiles, marked with stars in Fig. 8, are placed as expected. For example, the estimation of the profile for the orientation $p=30^\circ$ (marked with green stars), which was not part of the training set, is placed in between the profile for the pose $p=0^\circ$ (shown in blue) and the one for orientation $p=45^\circ$ (shown in red), and closer to the deformation profile of orientation 45° . The same for the estimation for orientation $p=80^\circ$ (marked with black stars) that is placed in between 75° (magenta profile) and 90° (cyan profile) and closer to orientation $p=75^\circ$. This example shows the modeling capability of the proposed neural network solution, not only to capture correctly existing data, but also to provide good estimates for data that were not part of the training set.

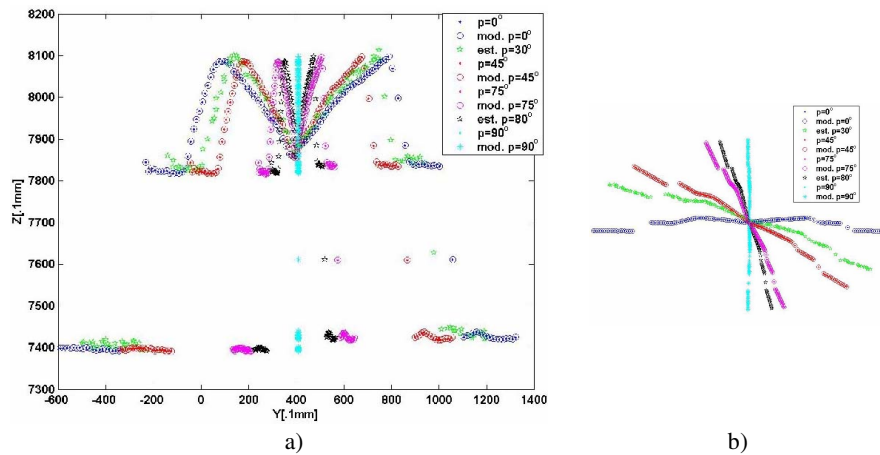


Fig. 8. Real, modeled and estimated deformation profiles at different orientations of the range finder under a constant force of $F=7.5N$, applied in the normal direction on point O : a) lateral view and b) top view

5 Conclusions

This investigation into means of modeling elastic behavior demonstrates that the benefit of using neural networks to model deformable objects is multi-folded. First, neural networks provide continuous output behavior, thus being able to provide the necessary nonlinear interpolation for estimates of data that was not part of the training set. When compared with most of the work found in the literature where *a priori* knowledge about the characteristics of the material is assumed available, this research work proposes a robust approach for modeling force/deformation relationships from realistic experimental data with noisy and incomplete measurements, the latter being exemplified here by missing values for some of the points along the scan line. Second, the use of a neural network modeling scheme avoids the complicated and frequently impossible to solve problem of recuperating explicit elastic parameters, especially for highly nonlinear elastic materials. Third, neural networks provide an accurate and fast response once they are trained. After the elastic behavior of an object is stored in a neural network, the latter can provide real-time information about the elasticity in any point of an object. Finally, the neural network modeling of deformation profiles captures naturally the modification of the objects' volume due to applied external forces.

Future research work is directed towards means to integrate the deformation profiles with 3D vision data into coherent models of objects to be used in virtualized reality applications.

References

1. Wang, X., Ananthasuresh, G.K., Ostrowski, J.P.: Vision-based Sensing of Forces in Elastic Objects. *Sensors and Actuators A* 94, 146–156 (2001)
2. Kamiyama, K., Kajimoto, H., Kawakami, N., Tachi, S.: Evaluation of a Vision-based Tactile Sensor. In: *IEEE International Conference on Robotics and Automation*, pp. 1542–1547. IEEE Press, Barcelona (2004)
3. Vuskovic, V., Krauer, M., Szekely, G., Reidy, M.: Realistic Force Feedback for Virtual Reality Based Diagnostic Surgery Simulators. In: *IEEE International Conference on Robotics and Automation*, pp. 1592–1598. IEEE Press, San Francisco (2000)
4. Ferrier, N.J., Brockett, R.W.: Reconstructing the Shape of a Deformable Membrane from Image Data. *International Journal of Robotics Research* 19(9), 795–816 (2000)
5. Hristu, D., Ferrier, N., Brockett, R.W.: The Performance of a Deformable-Membrane Tactile Sensor: Basic Results on Geometrically-Defined Tasks. In: *IEEE Conference on Robotics and Automation*, vol. pp. 508–513. IEEE Press, San Francisco (2000)
6. Greminger, M.A., Nelson, B.J.: Modeling Elastic Objects with Neural Networks for Vision-Based Force Measurement. In: *IEEE International Conference on Intelligent Robots and Systems*, vol. 2, pp. 1278–1283. IEEE Press, Las Vegas (2003)
7. Cretu, A.-M., Payeur, P., Petriu, E.M.: Neural Network Mapping and Clustering of Elastic Behavior from Tactile and Range Imaging for Virtualized Reality Applications. *IEEE Transactions on Instrumentation and Measurement* 57(9), 1918–1928 (2008)